Volume 1 | Number 1 | Jan 2013 | Pages 1–100

## Lab on a Chip

Miniaturisation for chemistry, physics, biology, materials science and bioengineering
www.rsc.org/loc

ROYAL SOCIETY OF CHEMISTRY

ROYAL SOCIETY OF CHEMISTRY

www.rsc.org/loc

39x19mm (300 x 300 DPI)

Please do not adjust margins
**Lab on a Chip**
Page 2 of 20

# Journal Name

## ARTICLE

### A 3D printed microfluidic device for production of functionalized hydrogel microcapsules for culture and differentiation of human Neuronal Stem Cells (hNSC)

Kevin Alessandri[a,b,c†], Maxime Feyeux[d†], Basile Gurchenkov[b,c,g,h,i], Christophe Delgado[d], Anastasiya Trushko[a], Karl-Heinz Krause[d], Daniela Vignjević[i], Pierre Nassoy[a,b,e,f], and Aurélien Roux[a,j]∗

We present here a microfluidic device that generates sub-millimetric hollow hydrogel spheres, encapsulating cells and coated internally with a layer of reconstituted extracellular matrix (ECM) of a few microns thick. The spherical capsules, composed of alginate hydrogel, originate from the spontaneous instability of a multi-layered jet formed by co-extrusion using a coaxial flow device. We provide a simple design to manufacture this device using a DLP (Digital Light Processing) 3D printer. Then, we demonstrate how the inner wall of the capsules can be decorated with a continuous ECM layer that is anchored to the alginate gel and mimics the basal membrane of a cellular niche. Finally, we used this approach to encapsulate human Neural Stem Cells (hNSC) derived from human induced Pluripotent Stem Cells (hIPSC), which were further differentiated into neurons within the capsules with negligible loss of viability. Altogether, we show that these capsules may serve as cell micro-containers compatible with complex cell culture conditions and applications. These developments widen the field of research and biomedical applications of the cell encapsulation technology.

## INTRODUCTION

Cells from a wide array of origins and phenotypes have been successfully cultured *in vitro*. While the standard method remains the Petri dish, there is now growing evidence that 2D cultures in a plastic dish present numerous limitations [1]. Firstly, Petri dish-based cultures are poorly suited to culture sampling and many downstream applications, for which cells need to be chemically or enzymatically detached from the substrate. This drastically restricts the range of possible experimental investigations. Secondly, they do not recapitulate the 3D architecture of tissues, which calls into question their ability to mimic the physiological functions of living tissues.

Over the past decade, different strategies have been pursued to develop 3D cell culture systems. Multicellular aggregates have been formed using techniques such as the hanging drop method, gyratory rotation or liquid overlay cultures [2]. These cellular spheroids have been extensively used as *in vitro* models of tumors, in particular for drug testing [3]. Recently, organoids of cerebral tissue derived from pluripotent stem cells have been proposed as mini-brain models since they recapitulate the primordial structure and gene expression programs of the cerebral cortex [4]. An alternative approach to 3D systems is to culture cells on and around synthetic degradable scaffolds [5] or biocompatible matrices, [6] such as hydrogels that permit oxygen and nutrient diffusion [7]. Even though remarkable achievements have been obtained, all these techniques lead to the production of 3D cultures that exhibit a wide variability in size, shape, structure and functional features. Moreover, they are not amenable to massive production and thus to automated manipulation for high throughput screening assays.

In this context, microfabrication and microfluidics technologies are expected to provide new approaches towards this goal and to allow further applications in tissue engineering and regenerative medicine. In particular, co-flow or co-extrusion micro-devices have been developed to generate hydrogel cell-enclosing spheres [8] or capsules with core-shell structures [9]. Using homemade and manually assembled glass devices, we have previously demonstrated how to produce calibrated tumor spheroids grown in hollow alginate capsules and to exploit the elasticity of the shell to measure the pressure exerted on it by the *in vitro* tumor growing within[10].

a. University of Geneva, Department of Biochemistry, quai Ernest Ansermet 30, CH-1211 Geneva 4, Switzerland.
b. Institut Curie et Centre National de la Recherche Scientifique, Unité Mixte de Recherche 168, F-75248 Paris, France.
c. Université Pierre et Marie Curie, F-75005 Paris, France.
d. Department of Pathology and Immunology, Faculty of Medicine, University of Geneva, CH-1211 Geneva 4, Switzerland.
e. Université de Bordeaux, LP2N, UMR 5298, F-33400 Talence, France.
f. Institut d'Optique & CNRS, LP2N, UMR 5298, F-33400 Talence, France.
g. ICI, IGBMC, CNRS, UMR7104, F-67404 Illkirch-Graffenstaden, France
h. INSERM, U964, Université de Strasbourg, F-67400 Illkirch-Graffenstaden, France.
i. Institut Curie et Centre National de la Recherche Scientifique, Unité Mixte de Recherche 144, F-75248 Paris, France.
j. Swiss National Centre for Competence in Research Programme Chemical Biology, 1211 Geneva, Switzerland.
†These authors contributed equally to this work.
*Corresponding author.
Electronic Supplementary Information (ESI) available: [details of any supplementary information available should be included here]. See DOI: 10.1039/x0xx00000x

However, one limitation of such co-extrusion techniques, which require the assembly of multiple co-axial capillaries, is the fabrication of the 3D microfluidic circuit itself, which allows sample injection and subsequent capsule formation. Soft lithography based techniques are not optimal for performing the sequential combination of fluid co-extrusion and gelation reactions. We therefore predicted that the recent development of 3D printing could provide a simple route to overcome this difficulty. The use of 3D printing-assisted micro-devices has indeed gained interest and popularity in the recent years. Even though most developments still aim at fabricating microstructures that eventually serve as molds for soft lithography [11], we may anticipate new prospects in microfluidics by integrating basic elements or fluid manipulation blocks into functional microfluidic devices such as T-junctions or mixers. 3D printing also offers the advantage of allowing rapid prototyping from design to manufacturing within less than a day. In this work we have exploited the capabilities of 3D printing to design a simple micro-injector for alginate capsule production. We managed to print channels of 200 μm in diameter by adapting the design to the working principle of the printer.

Another limitation of alginate-made cell carriers lies in the intrinsic physico-chemical properties of the hydrogel; cells do not adhere onto alginate surfaces. The fact that alginate gels exhibit ultra-weak affinity for proteins [12], and thus prevent the formation of a cell-adhesive substrate, limits their potential use to non-adherent cells. But most cell types, from endothelial, epithelial cells to neurons, as well as fibroblasts, require adhesion for proper tissue organization. Two main strategies have been pursued to overcome this difficulty. The first one involves chemically modifying the sodium alginate, *e.g.* by grafting peptidic residues with high affinity for cell-adhesion molecules to the polysaccharide backbone [13-15]. The second strategy is to mix alginate with Extra-Cellular Matrix solution (ECM) prior to gelation [16-18]. Here, we propose a third approach, which is to use the inner surface of the alginate shell as a template for the anchorage of an ECM layer, namely Matrigel.

Finally, we show that these technological developments allowed us to encapsulate Neuronal Stem Cells (NSCs), to differentiate them into neurons *in situ* and to perform long-term culture of the neuronal tissues. Fig. 1 shows a schematic depiction of the neuronal capsule that we produce. The alginate shell is protective. The Matrigel layer favors and supports the growth of hNSCs. The size of the capsule was selected to be in the order of 200 μm, which is known to be the diffusion distance of oxygen in biological tissues beyond which cells become hypoxic and start dying.

## RESULTS

### A 3D printing technique for rapid prototyping of microfluidics circuitry in biology

We previously designed and manually fabricated a 3-way co-extrusion device to produce capsules containing mammalian cells [10]. This method allows massive production of size-controlled permeable hollow spheres and seems to be versatile enough to allow for a plethora of biological applications. However, the remaining bottleneck for wider use was the fabrication of the device itself, which is time-consuming, impossible to replicate in an automated fashion and not optimized in terms of dead volume. This latter issue may indeed become critical when expensive biological species are used. We thus looked for other routes for producing similar co-extrusion devices.

This new approach takes advantage of fast developing 3D printing technology, which could be well adapted for standardized production of the co-extrusion device. 3D printing also decreases the time required to prototype microfluidic modules. Among the available 3D printing technologies, we chose a Digital Light Processing (DLP) printer (Pico27 from Asiga, USA), because of its good resolution (27 microns in XY) which *a priori* offers the possibility to print 200 μm wide channels in a block of resin.

However, resolution is not sufficient to ensure successful fabrication of channels or holes that are 10 times bigger in diameter so these intrinsic limitations of the DLP printing principle had to be overcome. Direct printing of a simple 200 μm channel perforating a 3 mm thick disc of radius 2.5mm (Fig. 2(A)), leads to a plain block with no visible channel (Fig. 2(B)). A small depression can only be detected in the center, the depth of which is approximately 50-70 μm. The discrepancy between the drawn 3D model and the actual printed piece originates from the very principle of DLP printing, in which i) a slicing program sections the 3D shape into a stack of 2D layers; ii) each layer is projected as a 2D image by a DLP, and the photo-polymerizable resin is cured in progressive layers of 25 microns thick. Thus, the light emitted by the printer to cure one layer may also affect the previous layers, resulting in partial unwanted curing of out of focus layers. Because the non-polymerized resin confined in the channel can be irradiated several times with UV light during subsequent steps, it finally gets polymerized (Fig. 2(C)). To overcome this difficulty, the obvious solution is to mix the liquid resin after each layer is printed in order to prevent it from stagnating. In the basic working principle of a DLP printer, the block of polymerized resin is detached from the bottom plateau, which effectively generates flows within the reservoir of liquid resin between the printed block and the bottom of the printing chamber. We combined this effect with a modified design of the channel to allow efficient washing of the channel that is being printed. In practical terms, this involved integrating a side exit into the printed piece with a 90° angle connecting it to the vertical channel (Fig. 2(D-E)). In this design, the separation between the solidified resin and the bottom plateau at each printing step creates a pressure difference between the printed face and the side exit. The suction force produced on the face of the printed face, aspirates fresh resin within the channel (Fig. 2(F)). Using this design, we could successfully obtain a continuous channel through the printed resin block (Fig. 2(E) right). Note that the stratified

Please do not adjust margins
**Lab on a Chip**
**Page 4 of 20**

structuration that is observed corresponds to the 25μm steps of the printing process.

With our previously published glass co-extrusion device, the multi component capsules were formed using a high flow-rate liquid jet that undergoes a Rayleigh-Plateau instability (see Materials and Methods for details). Cells are injected into the center zone isolated from the alginate solution by an intermediate buffer solution (sorbitol) (Fig. 3(A) and 3(B)). We designed the new co-extrusion device made by 3D printing (Fig. 3(C)), with the same basic design as the glass version [10]. The three inlets are located on the side of the device to favor renewal of the liquid resin during the printing process, as explained above. A magnification of a mechanical cut through the tip (Fig. 3(D)) reveals the three imbricated conical layers. Alginate is flowed into the channel connecting to the outer conical printed capillary.

To feed the back of each cone into the tip as homogeneously as possible, we designed a symmetrical circuit of 4 channels with distributed connections (see Supplementary Fig. 1). The size, and the design of these channels were chosen to keep the flow low and fairly constant within the device, to avoid liquid mixing at the nozzle exit (see supplementary Fig. 2). Finally, a slice of Teflon capillary is glued to the conical tip to ensure hydrophobicity and regularity of the hole (see Methods section for technical details), crucial parameters for stabilization of the jet flow and proper formation of capsules (Fig. 3(E)). The overall dead volume of the device is around 5μL, which is about 20 times smaller than for the hand-made glass device.

Finally, we studied the capsule size distribution produced by our device (Fig. 4A). Many capsules display small tails as already discussed in a previous paper [10]. The mean radius is 136±28 μm (SD). The size distribution is skewed towards low values, which suggests the occurrence of satellite capsules (Fig. 4B): as described in our previous work [10], the fraction of small capsules originates from the formation of satellite droplets that is a typical by-product in droplet microfluidics due to inter-droplet filament thinning. The fraction of larger capsules often results from the coalescence of two droplets during their fall before gelation, as evidenced by the observation of septa-like structures (Fig. 4A). The occurrence of coalescence events is lower than the one of satellite droplets generation. All capsules exhibit a roundness higher than 0.8 and 32% have a roundness higher than 0.9 (Fig. 4C). Note that the roundness (or shape factor) is computed from the micrographs and defined as $(a/b)^2$ where $a$ and $b$ are the short and long axes. Even though small capsules are often more spherical than larger ones due to a higher Laplace pressure, our main criterion for capsule selection was based on the capsule size. In the present work, we have further manually selected any a sub-population of these capsules, with inner diameter optimized for cell culture (outer diameter <130μm, in order to avoid possible appearance of necrotic core). By comparison with the first glass capillary-based version of the device [10], the fraction of capsules that can be further used for cell culture is higher. Whereas roundness is not improved (very likely due to intrinsic effects due to spontaneous Rayleigh instability and

impact onto the calcium bath), the poly-dispersity of the capsules has been significantly reduced.

**Engineering a microscopic coating of reconstituted Extra-Cellular Matrix**

As previously reported [12], alginate gels are protein- and cell-repellent. This property is an advantage for the compartmentalized growth of independent multicellular spheroids, as exploited for tumor cells [10]. However, in numerous other situations, cells require adhesive contact with a substrate to grow, *e.g.* for epithelial cells, endothelial cells, hNSCs or neurons. Matrigel, a protein mixture obtained from mouse sarcoma cells, is widely considered to resemble the basement membrane found in tissues. Our objective was to coat the inner wall of alginate capsules with a layer of Matrigel resistant to cell adhesion and traction forces. Two difficulties had to be overcome. First, alginate gelation is triggered by calcium ions while Matrigel gelation is temperature controlled (liquid at 4°C with gelation occurring between room temperature and 37°C). Second, alginate gel has a low affinity for proteins [12], which is *a priori* not favorable to Matrigel anchorage.

A natural route to design this bi-layered capsule was to use the intermediate input of the co-extrusion device to inject Matrigel, which will be squeezed between the flows of the alginate solution and cell suspension and to synchronize Matrigel gelation with alginate gel formation. To do so, Matrigel was kept in a liquid state at 4°C prior to injection using a customized temperature-control device (Fig 3(A)-(B) and see details in Methods section) to cool down the microfluidic circuit connecting the syringes to the co-extrusion device. Synchronization between temperature-induced gelation of Matrigel and calcium-mediated gelation of alginate was simply performed by using a hot (T= 37°C) calcium bath. This method also allowed us to use smaller volumes of Matrigel (<200μL) than the ones required to fill milliliter-sized syringes. Unfortunately, this approach repeatedly led to the formation of deformed capsules. We suspect that the Matrigel, which contains divalent salts, diffused too rapidly towards the alginate solution, and interfered with alginate polymerization. Counter-intuitively, we had to inject the Matrigel solution into the inner capillary (i.e. mixed with the cell suspension) to obtain a Matrigel layer underneath the alginate shell. At the optimal Matrigel concentration of 25% v/v a homogeneous layer of fluorescent laminin contained in Matrigel was deposited onto the inner wall of the alginate capsule, as seen in Fig. 5(B) and Supplementary Movie 1 (Fig. 5(E)). At 10% v/v (Fig. 5(A)), the Matrigel layer was highly discontinuous (Fig. 4(d)), suggesting an insufficient amount of material for complete coverage. Contrastingly, at a concentration of 40% v/v (Fig. 5(C)), the Matrigel layer was observed to be continuous underneath the alginate wall but supplemented with bulk Matrigel in the core of the capsule, suggesting an excess of Matrigel within the encapsulated material (Fig. 5(F)). Plotting the fluorescence gradient of alginate and Matrigel (Fig. 6(A)), shows that the two hydrogels are not juxtaposed

but do overlap, suggesting that they form interpenetrated networks. Quantitative measurements derived from radial scans show that the thickness of the continuous Matrigel layers was about 2.5-3 μm, independently of the initial concentration of Matrigel and of the alginate shell thickness (Fig. 6(B)). Despite the protein-repellent nature of alginate gels, the Matrigel layer was well anchored to the capsule shell. Although this situation is highly reproducible, the explanation for the entanglements between both gels remains unclear. Due to a viscosity contrast between the alginate solution and the inner solution, slight mixing at the interface cannot be ruled out, which may favor the formation of interpenetrated networks.

To further characterize this interpenetrating hydrogel structure, we also investigated the influence of the alginate shell thickness on the width of the alginate/Matrigel mixed layer. To do so, the ratio between inner and outer flow rates was varied as explained in previous work [10]. The thickness over which both gels were intermixed was measured from the fluorescence intensity profiles of the alginate and Matrigel layers (Fig. 6(A)). Remarkably, the thickness of the interpenetrating layer containing both Matrigel and alginate was observed to increase linearly with the alginate capsule thickness in a range of 1-5 μm (Fig. 6(C)). An oversimplified diffusion calculation may indeed yield such a linear relationship. By assuming that alginate crosslinking has faster kinetics than Matrigel gelation and is completed within time $T_{alg}$, the distance over which Matrigel molecular species may diffuse is $\lambda \sim (D_{Mat}.T_{alg})^{1/2}$ or equivalently $\lambda \sim (D_{Mat}/D_{Ca})^{1/2}.d$, with $D_{Ca}$ and $D_{Mat}$ the diffusion coefficients of calcium ions and Matrigel components respectively (in water), and $d$ the shell thickness. While $\lambda$ is found to be proportional to $d$, we are aware that this diffusion-based argument does not hold strongly since mixing and convection cannot be neglected during the impact of the droplet onto the surface of the calcium bath.

**Stem cells culture and differentiation into neurons inside the Matrigel-coated alginate capsules**

We tested whether our Matrigel-coated capsules could be effectively used as neuronal 3D culture systems. Cells to be encapsulated must be in a cell suspension, but human mature neurons cannot withstand any detachment or time spent in a liquid suspension. We bypassed this difficulty by encapsulating Neural Stem Cells (NSCs). These cells were derived from the BC1 hIPSCs line obtained from MTI-Globalstem using a previously published protocol [19]. Encapsulation was performed by adding 25% Matrigel to the cell suspension as described in the previous section. NSCs survival was assessed by fluorescence microscopy using classical viability dyes. The encapsulation step itself led to 97.7% (SD=1.8) survival rate (see Materials and Methods section for details). Capsules were then maintained in NSC proliferation medium for 72 hours after encapsulation, in order to allow confluency to be reached. When capsules were filled with cells, we implemented the classical protocol for spontaneous neuronal

differentiation in a Petri dish, i.e. by replacing the medium with a mitogen-free medium. After 13 days of growth? in the differentiation medium, no neuronal network formation signature could be visualized within the cellular capsules by phase contrast microscopy (Fig. 7(A)). To gain insight into the cell content, we performed fluorescence staining with specific antibodies. Capsules were treated with 4% paraformaldehyde (PFA) in phosphate buffered saline (PBS), which both fixed cells and dissolved the alginate shell. Confocal imaging and 3D reconstitution was then performed on fixed samples. DAPI immunostaining first revealed that cells are densely packed with very little nuclear debris (Fig. 7(B)). More surprisingly, Beta3 tubulin staining revealed an entangled 3D network of neurons neurites, rich in tubulin (Fig. 7(C)), which is a clear-cut signature that differentiation of NSCs into neurons occurred within the capsule.

Other classical neural progenies markers were further tested to confirm that NSCs were successfully and efficiently differentiated. Most cells expressed the Microtubule Associated Protein 2 (MAP2) and the RNA binding protein HuD/ELAVL4, a nucleic marker expressed only in neurons, (Supplementary Fig. 3(a) and 3(b)). A subset of the cells expressed the synapsin1 axonal/synaptic phosphoprotein, a further indication of neuronal maturation (Supplementary Fig. 3(a)). A significant subset of cells still expressed the intermediate filament Nestin, expressed by progenitor cells (Supplementary Fig. 3(c)). A very small amount of cells expressed the astrocyte/radial glial cell intermediate filament marker GFAP (Supplementary Fig. 3(c)). Precise estimation of the percentage of the different subsets of cells would require a series of more detailed biological assays and image analyses, which goes beyond the scope of the present work.

We were, however, able to carry out a quantitative viability analysis. Viability was estimated from confocal stacks of the DAPI immunofluorescence images (see Materials and Methods for details). Picnotic nuclei, which are typical of apoptotic cells can indeed be distinguished from intact nuclei on the basis of size and structuration criteria. They also have a brighter DAPI fluorescence and are smaller (10-20 μm2 as compared to 100-200 $\mu m^2$ in projected area) than intact nuclei. Image analysis for more than 10 capsules corresponding to ~20,000 cells, indicates a viability of 97.8% (SD=1.4) after 2 weeks of differentiation inside the capsules.

Finally, we aimed to perform live imaging of cell phenotypic transition from self-renewing NSCs to post-mitotic neurons. Since high cellular density prevents any visualization by label-free microscopy we decided to trigger differentiation prior to confluence. As can be seen in supplementary Video 2, encapsulated 3D cultures showed a marked phenotypic transition starting at eight days after encapsulation, with cell bodies moving along expanding cellular processes. As capsules matured, neurite outgrowth became more prevalent and axonal growth cones were seen crawling on the Matrigel layer.

## DISCUSSION

We have presented a novel strategy for generating 3D neuronal networks. The method builds on the recently developed cellular capsule technology [10], and is improved in terms of simplicity and versatility (and reproducibility) of the implementation. We have first described the design and the fabrication steps of a new 3D printed co-extrusion device that allows cell encapsulation within hydrogel hollow spheres and 3D cell culture. PDMS-based droplet microfluidics has been widely used to produce bulk particles, with extensions to double emulsification yielding core-shell capsules (see review [20]). In the case of permeable hydrogel shells, the crosslinking agent required for gelation is generally dissolved in oil used as a continuous phase. This approach has been successfully executed to produce cells enclosed in alginate shells [9, 21]. These methods usually generate monodisperse and perfectly spherical capsules. However, practically, when cells were suspended in the culture media, the inner walls of the capsules were observed to exhibit irregular shapes. Increasing the viscosity of the cell suspension through addition of glycerol improved the capsule shape but led to drastic reduction of cell viability (below 10%). An alternative to soft lithography involved using a glass micro-capillary device, as originally proposed by Utada and colleagues [22] and recently adapted for 3-way co-extrusion [10]. This approach required manual assembly with exquisite care in the alignment of the concentric capillaries. Similar devices were implemented using metallic syringes under high DC voltage to trigger the jetting instability [23, 24]. The main advantage offered by our 3D printed device is to overcome the difficulties encountered in the manual assembly of capillaries.

The 3D printer that we used is based on a standard HD video projector and has a lateral resolution of 27 µm. However, as explained in the present work, the nominal resolution is not always the limiting factor. Resin polymerization out of the plane of irradiation may be highly detrimental when narrow channels need to be manufactured. At the onset of the present work, the lower limit for prototyped channels using a DLP printer was 500-750 µm in diameter [25]. We show that we can scale them down to about 200 µm in diameter, provided that the overall circuitry is carefully designed.

Then, by refining the working principle of the technology, we show how the inner wall of the capsule can serve as a template for ECM coating. In previous studies [26], to restore cell adhesion on alginate surfaces, alginates were chemically modified via grafting of peptidic residues with high affinity for cell-adhesion molecules to the polysaccharide backbone [13-15], or mixed with ECM solution prior to gelation [16-18]. In the latter case, as well as a modification of the gel structure and resistance, the superior immuno-protective effect provided by pure alginate is expected to be impaired for implantation applications. Moreover, all of these works were focused on bulk alginate or plain beads. Recently, Ma and co-workers have reported the formation of alginate capsules enclosing bulk ECM, including Matrigel, collagen or fibrin [27]. By contrast, our work is characterized by two specificities. First, cells are encapsulated in a pure alginate hollow capsule, thus preserving its immuno-protective properties on the outer

surface. Second, a minimal amount of exogenous ECM is introduced; the micrometric surface coating only serves to promote adhesion. The Matrigel layer anchored to the inner wall of the capsule can be envisioned as an *in vitro* basal membrane. The typical size of the capsules was about 100 µm in radius. This upper limit, which matches the maximum capillary to neuron distance in the human cortex [28], prevents core necrosis in a non-vascularized *in vitro* setup.

The formation of encapsulated neuronal networks was achieved in two steps. First, we differentiated human Induced Pluripotent Stem Cells (hIPSCs) into Neural Stem Cells (NSCs) using published protocols [19]. Second, NSCs were encapsulated in sodium alginate shells coated with Matrigel and further differentiated into neurons *in capsulo*, showing the compatibility of our method with complex cell differentiation protocols required for tissue formation *in vitro* [29]. The neuronal micro-tissues that we generated with the presented technology are further protected by the capsule and proved resilient to stirred liquid suspension culturing and repeated micropipette liquid handling.

Finally, we would like to discuss the biomedical potentialities of our technology. To our knowledge, the development of controlled 3D human neuronal networks has never been reported to date. Such a 3D culture system could, for example, be directly applied to neurotoxicity assays. The neurosphere is a 3D model that is currently often used for neuronal differentiation [30]. This model is a spontaneous spherical aggregate of poorly controlled size, typically >400µm in diameter, and thus exhibiting a necrotic core. This model was recently improved based on a hydrogel well technique with neural cells harvested on postnatal rat brains [31]. However, the use of human fetal neuronal tissues is unsustainable for human models due to ethical and availability concerns [31]. The source of choice for human neurons *in vitro* is neuronal stem cells. Furthermore, hIPSCs can be obtained from any individual by "reprogramming" differentiated cells to an embryonic state by means of artificial expression of four transcription factors - Oct4, Sox2, cMyc, Klf4 [32] - and allow both immuno-compatibility and scalability [33]. Additionally, neuronal differentiation protocols based on hNSC derived from hIPSCs allows for the manipulation of more resilient progenitors and subsequent differentiation to be performed *in situ*. All these protocols require a laminin-rich coating [19]. Thanks to our new cell culture container, we have been able to simply transfer the differentiation protocols from coated Petri dish (2D) to internally coated alginate capsules (3D). Remarkably, we obtained this differentiation with a very high density of cells and a final viability of >97%, probably due either to a very good survival rate or phagocytosis of cell debris as observed *in vivo* [34-36]. We were able to obtain a differentiation quality of progenitors at least as good as established protocols and within the same time frame. This is a proof of concept of a possibly rapid integration of existing stem cell protocols into more structured 3D tissue models.

More broadly, a major focus in bioengineering has been to generate functional human tissues *in vitro*. For this task, reconstituting tissue architecture and cell microenvironment is

essential, but tissue engineering based on the assembly of living cells and biological substrates is still challenging [37, 38]. This difficulty is even more striking for neuronal models. The most relevant models to date are organoids, based on stem cell differentiation either in bulk Matrigel [4] or in sophisticated scaffolds [39]. Our technology allowed us to produce similar neuronal organoids and to further reduce their fragility (due to the protective shell), restrict their size variability and increase drastically their production rate. We expect this technology to be instrumental in extending the field of application of *in vitro* organoïd generation and regenerative medicine.

Please do not adjust margins
**Lab on a Chip**
**Page 8 of 20**

## Experimental procedures

### 3D printing of the co-extrusion Device

The desktop 3D printer, Asiga pico27, was used in conventional working condition and factory settings for all printing parameters except "normal exposure" time set at 0.7 second and "burn-in-layer exposure time" at 5 seconds. Prints were made with the Asiga plastclear resin and typically take around 40 minutes. The print was then rinsed with ethanol. Extensive rinsing helps remove liquid resin from the inner channels. Rinsing must however be gentle to avoid degradation of the thin walls before curing. The print was then cured for 30-60 min in the Asiga curing chamber. Three 19-gauge stainless steel segment of 1 cm (with ground extremities) were then glued with epoxy resins (Loctite M-31cl medical device) in the inlets as connectors. Since capsule shape depends on the regularity of the jet exiting the co-extrusion device, a smooth and hydrophobic tip was observed to be crucial. The inner diameter of the nozzle was around 100μm to produce capsules with a diameter of about 200μm. At the tip, any defect bigger than 5 μm would lead to a beating jet and poor capsule quality. In a previous version of the device, the tip was a glass capillary, which was pulled and ground by hand with a piece of diamond paper followed by a hydrophobization using standard silane chemistry. Use of Teflon capillary PFA HP PLUS TUBING, 360μm OD, 100 μm ID from IDEX) is simpler and more reproducible. We cut it into sections of 400μm with a scalpel blade. The hole in the printed tip is 200μm in diameter and the Teflon capillary section is centered within a positioning ring of 500μm in diameter. The Teflon capillary section is glued using a small drop of epoxy resin directly on the positioning ring. The device was ready for use after complete polymerization of the epoxy resins, i.e. after 24 hours at room temperature. To ensure proper functioning for several runs of encapsulation, the device should never be washed with organic solvent such as ethanol or autoclaved. Sterilization is performed instead by rinsing the device with Biocidal ZF from Biovalley.

The design has been optimized to avoid errors while printing. The structure has to withstand by itself, and sustain the flow of resin and the mechanical stress resulting from the peeling of the print from the bottom of the construction tray. The 60° angle and the 200μm walls (8 pixels wide) ensure reduced turbulence when the flows join to form the mixed jet.

### Human IPS Cell Culture

BC-1 (WT XY, passages 5-14, MTI-Globalstem, Maryland, USA) induced pluripotent stem cell line was maintained under feeder free conditions. Culture plates were coated with Matrigel® matrix (Corning, #354248, New York, USA, 1/100 in DMEM medium, 2 hours at 37°C). BC-1 colonies were routinely sub-cultured using GCDR (gentle cell dissociation reagent, # 07174, Stemcell technologies, France). The pluripotent stem cells were cultured in Nutristem XF (Stemgent, medium complemented with 1% penicillin/streptomycin Invitrogen). Cultures were fed daily and passaged every 5-7 days.

### Human IPS Cell Neural Induction

Neural differentiation was performed as described in 9 with some modifications. BC-1 PS cell cultures were washed once in PBS then ES cell medium was changed for the differentiation medium composed of N2B27 medium 31 supplemented with FGF2 (5ng/ml). BC-1 PS cells were detached from the Matrigel® matrix, collected in N2B27 and transferred for 6 hours to a non-coated Petri dish in order to remove feeders' contamination. Cells were then seeded on Poly-ornithine and Laminin (Sigma, St. Louis, Missouri, USA) coated tissue culture multiwell plates. Differentiation medium was changed after 24h then every other day. LDN-193189 (500nM, Stemcell Technologies, Grenoble, France) and SB431542 (20μM, Tocris Biosciences, Ellisville, Missouri, USA) were added from day 0, then in every medium change. At day 8 to 12 rosettes arose in the dish.

### Neural Stem Cells Isolation

Neural Stem Cells isolation was performed as described in [19] with some modifications. Rosettes obtained were collected at day 10-14 from neural induction protocol, detached using GCDR and seeded at $10^5$ cells/cm² in Poly-ornithine and Laminin (Sigma, St. Louis, Missouri, United States) coated tissue culture plates in N2B27 medium supplemented with FGF2 (10ng/mL Invitrogen, Cergy Pontoise, France), EGF (10ng/mL R&D systems, Minneapolis, USA) and BDNF (10ng/mL Peprotech, London, UK). Cells were maintained in the same medium and passaged every 2-3 days until passage 20 at which they were discarded.

### Encapsulation Procedure

Two of the fluid phases (Intermediate solution (IS), and AL; Fig. 3) were loaded directly into syringes (10MDR-LL-GT SGE; Analytical Science) fitted to tubings (0.5mm ID; Bohlender) with P-678 (1/4''-28 FEM TO FEM LUER TEFZEL) and P-201 (Flangeless Male Nut Delrin®, 1/4-28 Flat-Bottom, for 1/16" OD Black) and P-200X (FLANGELESS FERR 1/16'' BLUE) from IDEX. The loading of the third fluid phase CS is detailed below in the sub-section "Matrigel microfluidic thermostated device". The other ends of the tubings were inserted into the appropriate inlets of the co-extrusion device, which is clamped vertically to a post inside a laminar flow hood. The syringes were mounted on syringe pumps (neMESYS low pressure module V2). In this work, we mostly used one set of flow rates: qCS=20mL·h-1, qIS=20mL·h−1, and qAL=30mL·h−1. After initiation of the flows (blowing air on the tip might be necessary to start the jetting), the compound microdroplets are directed to a gelation bath containing 100mM calcium chloride (VWR International) and traces of Tween 20 surfactant (Merck) deposited at the air liquid interface of the calcium bath with the tip of a sterile needle. The distance between the tip of the device and calcium bath was about 50cm. Operation for a few seconds was sufficient to produce several $10^4$ capsules, which were immediately sieved with 70μm Falcon Cell Strainers, washed in media without serum (to avoid precipitation) and transferred to the appropriate culture medium within less than 5 min. After use, the micro fluidic device was cleaned with disinfectant (Biocidal ZF; Biovalley) and deionized water.

**Matrigel Microfluidic Thermostated Device**

The device, which is seen in Fig. 3(a), is based on existing microfluidic tubing for HPLC. Two 4-way valve with a right angle "L" flow (fIDEX, V-101L) are mounted on the top of a copper plate (5X50X100mm). When the device is seen from the back and starting from the syringe (10MDR-LL-GT SGE; Analytical Science) a Teflon tube (0.5mm i.d.; Bohlender) of approximately 40cm is connected to the syringe with adaptors (from Idex P-678 & P-218). This tube is connected to the lower inlet of the right valve. From the upper inlet of the right valve a Teflon tube of 5cm is connected to a 1mL syringe. The left inlet of the right valve is connected to the right inlet of the left valve with a 30 cm Teflon tube wrap on the copper plate (this will be the cooled reservoir). The lower inlet of the left valve is connected to the co-extrusion device by a 5cm Teflon tube. A P-218 element is mounted without tube in the upper inlet of the left valve as a sample delivery cupule.

After careful cleaning (or autoclaving) the device is filled with sorbitol solution. Attention must be paid to avoid bubbles. It is then inserted in melting ice. For loading, the valves are rotated to allow the 1mL syringe to be in line with the sample delivery cupule (upper inlet of left valve) through the 30 cm Teflon tube immerged in ice. The sample (typically 200μL) is then filled into the sample delivery cupule and aspired into the 30cm long Teflon tube with the 1mL syringe. Valves are then rotated back to the working position where the 10mL syringe filled with sorbitol is in line with the 30cm tube in ice and the inlet to the co-extrusion device. The encapsulation procedure is then performed as described in [10]. The thickness of the capsule shell was varied by tuning the flows rates of the inner and outer solutions.

**Solutions and Cell Suspension Preparation**

The outermost phase (AL) was prepared by dissolving 2% wt/vol sodium alginate (Protanal LF200S; FMC) in water and by adding 0.5mM SDS surfactant (VWR International) as described previously7. The solution was filtered at 1μm (glass filters, Pall Life Science) and stored at 4 °C. The intermediate phase (IS) was a 300-mM sorbitol (Merck) solution. The innermost phase (CS) is a suspension of BC-1 neural stem cells that were detached using an enzyme-free cell dissociation buffer (GCDR, Stemcell technologies), re-suspended at $2.10^6$ cells/mL in sorbitol solution and mixed with Matrigel.

**Capsules Morphometric Measurements**

For confocal imaging of empty capsules. Matrigel was mixed at 10% with red-fluorescent laminin (REF LMN01, cytoskeleton Inc.). Fluorescent alginate (labeled with Alexa-488-TFP, Ref A-30005, Invitrogen) was added at 1% in AL solution. Image analysis was performed using ImageJ. Polar Transformer ImageJ plugin was used to convert a confocal image of a capsule taken at the equator to a straight line and measure the fluorescence intensity along the perimeter of the capsule. This transformed image was then linearly analyzed along the line (width: 10 pixels) through the Matrigel layer. A sliding median window of 25 pixels was then applied.

**Cell Viability Assessment and Cell Counting**

Cell viability was assessed in all cases on cell suspension using LIVE/DEAD kit (Ref L-3224, Invitrogen) and then imaged in epifluorescence using a 20X/NA=0.4 on an Evos FL (Thermo Fisher). Cells were then counted using standard ImageJ routines (thresholding and analyze particles). Then only particles matching size and roundness of cells were considered. Viability was successively assessed: i) in the Petri dish prior detachment of cells (95.3%), ii) in suspension prior to encapsulation (94.9%) and iii) after encapsulation and subsequent dissolution of the shell using PBS solution (92.7% with n=1839). Hence, as indicated in the main text, the viability from cell suspension to encapsulation is 97.7%.

**Immunostaining**

Cells were fixed directly in culture vessels with 4% PFA in Phosphate Buffered Saline (PBS, Thermofisher scientific 20012-027) for 1h (Capsules on uncoated glass bottom 96 well plate, CORNING, #4580) at room temperature (RT), washed twice with PBS and stored at 4°C. Capsules were left to settle in wells for 5 mins between each pipetting. For staining, slides were blocked with PBS+0.1% Triton X-100 (VWR) + 5% human serum (Sigma, H4522) for 1h at RT, incubated with primary antibodies overnight at 4°C (GFAP: Chemicon MAB360 1/250; Nestin: Millipore ABD69 1/2000; MAP2 Millipore MAB3418 1/250; Synapsin1 Chemicon AB1543P 1/250; HuC/D Molecular Probes A21272 1/100; beta3tubulin Covance PRB435P 1/1000), washed twice with PBS, incubated with secondary antibody incubation for 1h at RT, incubated with Dapi (1/10.000 in PBS) for 1h at RT and washed twice with PBS. For imaging, samples were imaged directly in the glass bottom 96 well plates.

**Confocal imaging**

Confocal images of the empty Capsules (with fluorescent alginate and red-fluorescent laminin loaded Matrigel) were obtained using upright LSM710 NLO microscope (Carl Zeiss) 40X/1-N.A. with water immersion objective (Carl Zeiss) directly in the Petri dish. Confocal images of the 3D samples were obtained using inverted LSM780 NLO microscope (Carl Zeiss) 40X/1-N.A. water immersion objective (Carl Zeiss) directly in the glass bottom 96 well plate.

**Long term *in vitro* Imaging**

A Biostation from Nikon was used to acquire contrast phase images (20X/ NA=0.4 and a full HD CCD camera) with a time interval of 5 min for up to two weeks. Culture medium was changed after one week. The Capsules were mounted using a home-made glass bottom dish. This dish was a 35mm plastic Petri dish. A hole was drilled in the center of the bottom of 1cm in diameter. A coverslip was glued to the bottom using epoxy resin. A larger Petri dish (50mm) was then hollowed to make a small reservoir around this Petri dish. The accessible surface of the coverslips at the bottom of the Petri dish was covered by a thin layer of 1% low melting point agarose (Invitrogen). The outer reservoir was filled with sterile water and the inner reservoir with media covering the layer of

solidified agarose. Capsules (typically 50) were then mounted using forceps (Dumont 5) by blocking them under a scale of agarose. A 50mm coverslip is finally positioned on top as a lid.

**Figures Legends:**

Fig. 1: Schematic depiction of a neuronal capsule.

Fig. 2: Overcoming 3D printing limitations: A. Computer-Assisted Design (CAD) of a single channel of 200 μm in diameter perforating through a cylindrical block. B. Print of the CAD presented in A, containing a dimple instead of a channel. C. Schematic of a transversal cut through the printed part presented in A just after illumination, for three subsequent layers (blue arrows and lines). Pink: photo-polymerized resin. Black lines: limits of the print according to the CAD. Green: partially photo-polymerized resin. D. CAD of a 90° angle channel. E. Print of the CAD presented in D. F. Schematic of a transversal cut through the printed part presented in D just after illumination, for three subsequent layers (blue arrows and lines) Pink: photo-polymerized resin. Black lines: limits of the print according to the CAD. Green: partially photo-polymerized resin. Dark grey arrow: flow of the liquid resin through the channel while the block is moving up to print the next layer. This flow flushes the partially polymerized resin (in green) in between illuminations. Scale bars 1mm.

Fig. 3: Principle and operation of the encapsulation set-up for the production of capsules coated internally with a Matrigel layer. A. Picture of the set-up. B. Diagram of the co-extrusion set-up; Pump: set of 3 syringe pumps for flow control, Valve: Home-made thermostated device for Matrigel injection. AL, Alginate Solution, IS, Intermediate Solution and CS, Cell Suspension. Coex: 3D printed co-extrusion device, $Ca^{2+}$: calcium gelation bath. Here, cells suspension is supplemented with liquid Matrigel. C. Photograph of the 3D printed co-extrusion device, scale bar 5mm, D. Close-up view of the co-extrusion device cut through the tip to display the internal circuitry, scale bar 500μm. E. Photograph of alginate capsules generated with the set-up shown in A, scale bar 1mm.

Fig. 4: Capsule morphometric measurements. A. Representative phase contrast micrographs of alginate capsules. Scale bar=200 μm. B. Capsule radius distribution. C. Capsule roundness distribution.

Fig. 5: Conditions for the formation of Matrigel-coated capsules. A-C. Confocal images of the equatorial plane of a representative capsule formed with: 10% (A), 25% (B), and 40% (C) of Matrigel as volume fractions in the core. Scale bar 10μm. D-F Curvilinear scans along circular contours through the Matrigel layer (in red) and at mid-distance from the center (in grey) providing plots of the normalized fluorescence intensity I as a function of the curvilinear coordinate s respectively at 10% (D), 25% (E), 40% (F) of Matrigel as volume fractions in the core.

Figure 6: Characterization of the Matrigel layer. A. Averaged radial profiles measured from confocal images of a capsule for the Matrigel layer (red) and the alginate shell (green). Shaded areas underline the extent of the pure Matrigel layer inside the

capsule (red), the thickness of the alginate shell (green) and the zone in which Matrigel and Alginate overlap (brown), suggesting the formation of interpenetrating polymer networks. B. Thickness of the pure Matrigel layer versus thickness of the alginate shell. C. Thickness of the Matrigel/alginate intermixed layer (brown in A) versus thickness of the alginate shell (green in A). Measured thicknesses in B and C are taken for fluorescence intensity I>0.2 Imax.

Fig. 7: Micrographs of a fixed neuronal capsule by bright field microscopy (A) and by fluorescence confocal microscopy (B-C) with DAPI staining of the nuclei (B) and with tubulin subunit Beta3 staining of mature neurites (C). Note that PFA treatment for fixation dissolves the alginate gel (not visible here). Scale bar 50μm

Supplementary Fig. 1: Internal structure of the co-extrusion device. In blue AL in green IS and in orange IS.

Supplementary Fig. 2: Flow simulations within the 3D printed co-extrusion device. Using the flow simulation function of solid works, we simulated the flow for the 3 inputs of the devices, with entry values according to the experimental parameters: A- entry flow 30 ml/h for Alginate Solution (AS), B- entry flow 20ml/h for Intermediate Solution (IS) and C- entry flow 20ml/h for Cell Solution (CS). As seen from the color code, the flow through the device stays low and fairly constant for all three inputs.

Supplementary Fig. 3: A. DAPI, Microtubule Associated Protein 2 (MAP2) marker for mature neurites and synapsin marker for mature synapses. Confocal images of Capsules fixed with PFA: B, DAPI, HUCD nucleic marker expressed only in neurons, the RNA binding protein HuD/ELAVL4 and tubulin subunit Beta3 marker for neurites of mature neurons. C, DAPI, GFAP marker for glial cells and Nestin marker for progenitors (non-differentiated NSCs). D. DAPI and control secondary antibodies in both channels red and green. Scale bar 50μm

Supplementary movie 1: 3D rendering of the Matrigel layer of a quarter of a capsule, based on 3D confocal imaging of a single capsule made with 25% of Matrigel as volume fractions in the core.

Supplementary movie 2: 13-day time-lapse phase contrast imaging of neuronal differentiation starting one hour post encapsulation of hNSCs within a capsule formed with 25% of Matrigel as volume fractions in the core.

## Acknowledgements

Please do not adjust margins
**Lab on a Chip**
**Page 12 of 20**

## Notes and references

1. B. M. Baker and C. S. Chen, *J Cell Sci*, 2012, **125**, 3015-3024.
2. J. B. Kim, R. Stein and M. J. O'Hare, *Breast Cancer Res Treat*, 2004, **85**, 281-291.
3. L. B. Weiswald, D. Bellet and V. Dangles-Marie, *Neoplasia*, 2015, **17**, 1-15.
4. M. A. Lancaster, M. Renner, C. A. Martin, D. Wenzel, L. S. Bicknell, M. E. Hurles, T. Homfray, J. M. Penninger, A. P. Jackson and J. A. Knoblich, *Nature*, 2013, **501**, 373-379.
5. J. S. Miller, K. R. Stevens, M. T. Yang, B. M. Baker, D. H. Nguyen, D. M. Cohen, E. Toro, A. A. Chen, P. A. Galie, X. Yu, R. Chaturvedi, S. N. Bhatia and C. S. Chen, *Nat Mater*, 2012, **11**, 768-774.
6. C. Fischbach, R. Chen, T. Matsumoto, T. Schmelzle, J. S. Brugge, P. J. Polverini and D. J. Mooney, *Nat Methods*, 2007, **4**, 855-860.
7. A. D. Augst, H. J. Kong and D. J. Mooney, *Macromolecular Bioscience*, 2006, **6**, 623-633.
8. S. Utech, R. Prodanovic, A. S. Mao, R. Ostafe, D. J. Mooney and D. A. Weitz, *Adv Healthc Mater*, 2015, **4**, 1628-1633.
9. C. Kim, S. Chung, Y. E. Kim, K. S. Lee, S. H. Lee, K. W. Oh and J. Y. Kang, *Lab Device*, 2011, **11**, 246-252.
10. K. Alessandri, B. R. Sarangi, V. V. Gurchenkov, B. Sinha, T. R. Kiessling, L. Fetler, F. Rico, S. Scheuring, C. Lamaze, A. Simon, S. Geraldo, D. Vignjevic, H. Domejean, L. Rolland, A. Funfak, J. Bibette, N. Bremond and P. Nassoy, *Proc Natl Acad Sci U S A*, 2013, **110**, 14843-14848.
11. C. N. LaFratta, L. Li and J. T. Fourkas, *Proc Natl Acad Sci U S A*, 2006, **103**, 8589-8594.
12. K. Y. Lee and D. J. Mooney, *Prog Polym Sci*, 2012, **37**, 106-126.
13. B. D. Plouffe, M. A. Brown, R. K. Iyer, M. Radisic and S. K. Murthy, *Lab Device*, 2009, **9**, 1507-1510.
14. E. Alsberg, K. W. Anderson, A. Albeiruti, R. T. Franceschi and D. J. Mooney, *J Dent Res*, 2001, **80**, 2025-2029.
15. L. Zieber, S. Or, E. Ruvinov and S. Cohen, *Biofabrication*, 2014, **6**, 024102.
16. Y. Wang and J. Wang, *Analyst*, 2014, **139**, 2449-2458.
17. R. C. de Guzman, E. S. Ereifej, K. M. Broadrick, R. A. Rogers and P. J. VandeVord, *J Microencapsul*, 2008, **25**, 487-498.
18. R. Yao, R. Zhang, J. Luan and F. Lin, *Biofabrication*, 2012, **4**, 025007.
19. M. Feyeux, F. Bourgois-Rocha, A. Redfern, P. Giles, N. Lefort, S. Aubert, C. Bonnefond, A. Bugi, M. Ruiz, N. Deglon, L. Jones, M. Peschanski, N. D. Allen and A. L. Perrier, *Hum Mol Genet*, 2012, **21**, 3883-3895.
20. S. Seiffert, *Chemphyschem*, 2013, **14**, 295-304.
21. J. K. Park and H. N. Chang, *Biotechnol Adv*, 2000, **18**, 303-319.
22. A. S. Utada, E. Lorenceau, D. R. Link, P. D. Kaplan, H. A. Stone and D. A. Weitz, *Science*, 2005, **308**, 537-541.
23. J. Lahann, *Small*, 2011, **7**, 1149-1156.
24. H. Chen, Y. Zhao, Y. Song and L. Jiang, *J Am Chem Soc*, 2008, **130**, 7800-7801.
25. K. C. Bhargava, B. Thompson and N. Malmstadt, *Proc Natl Acad Sci U S A*, 2014, **111**, 15013-15018.
26. J. A. Rowley and D. J. Mooney, *J Biomed Mater Res*, 2002, **60**, 217-223.
27. M. Ma, A. Chiu, G. Sahay, J. C. Doloff, N. Dholakia, R. Thakrar, J. Cohen, A. Vegas, D. Chen, K. M. Bratlie, T. Dang, R. L. York, J. Hollister-Lock, G. C. Weir and D. G. Anderson, *Adv Healthc Mater*, 2013, **2**, 667-672.
28. H. Duvernoy, S. Delon and J. L. Vannson, *Brain Res Bull*, 1983, **11**, 419-480.
29. G. M. Thomsen, G. Gowing, S. Svendsen and C. N. Svendsen, *Exp Neurol*, 2014, **262 Pt B**, 127-137.
30. J. Mokry, D. Subrtova and S. Nemecek, *Sb Ved Pr Lek Fak Karlovy Univerzity Hradci Kralove*, 1995, **38**, 167-174.
31. Y. T. Dingle, M. E. Boutin, A. M. Chirila, L. L. Livi, N. R. Labriola, L. M. Jakubek, J. R. Morgan, E. M. Darling, J. A. Kauer and D. Hoffman-Kim, *Tissue Eng Part C Methods*, 2015, **21**, 1274-1283.
32. K. Takahashi and S. Yamanaka, *Cell*, 2006, **126**, 663-676.

33.  J. Barry, J. Hyllner, G. Stacey, C. J. Taylor and M. Turner, *Curr Stem Cell Rep*, 2015, **1**, 110-117.
34.  R. W. Oppenheim, *Annu Rev Neurosci*, 1991, **14**, 453-501.
35.  D. Thomaidou, M. C. Mione, J. F. Cavanagh and J. G. Parnavelas, *J Neurosci*, 1997, **17**, 1075-1085.
36.  Y. Yamaguchi and M. Miura, *Curr Top Dev Biol*, 2015, **114**, 159-184.
37.  S. N. Bhatia and D. E. Ingber, *Nat Biotechnol*, 2014, **32**, 760-772.
38.  V. van Duinen, S. J. Trietsch, J. Joore, P. Vulto and T. Hankemeier, *Curr Opin Biotechnol*, 2015, **35**, 118-126.
39.  M. D. Tang-Schomer, J. D. White, L. W. Tien, L. I. Schmitt, T. M. Valentin, D. J. Graziano, A. M. Hopkins, F. G. Omenetto, P. G. Haydon and D. L. Kaplan, *Proc Natl Acad Sci U S A*, 2014, **111**, 13811-13816.
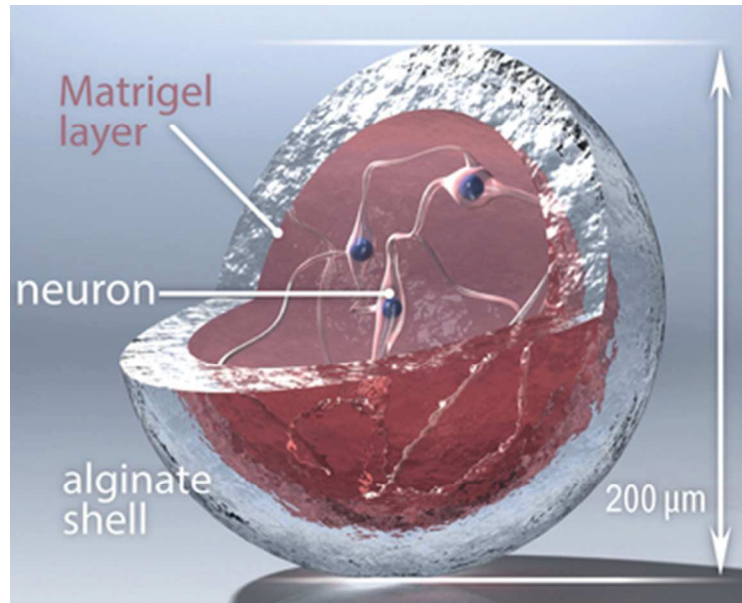
Fig. 1: Schematic depiction of a neuronal capsule.
31x25mm (300 x 300 DPI)

Fig. 2: Overcoming 3D printing limitations: A. Computer-Assisted Design (CAD) of a single channel of 200 µm in diameter perforating through a cylindrical block. B. Print of the CAD presented in A, containing a dimple instead of a channel. C. Schematic of a transversal cut through the printed part presented in A just after illumination, for three subsequent layers (blue arrows and lines). Pink: photo-polymerized resin. Black lines: limits of the print according to the CAD. Green: partially photo-polymerized resin. D. CAD of a 90° angle channel. E. Print of the CAD presented in D. F. Schematic of a transversal cut through the printed part presented in D just after illumination, for three subsequent layers (blue arrows and lines) Pink: photo-polymerized resin. Black lines: limits of the print according to the CAD. Green: partially photo-polymerized resin. Dark grey arrow: flow of the liquid resin through the channel while the block is moving up to print the next layer. This flow flushes the partially polymerized resin (in green) in between illuminations. Scale bars 1mm.
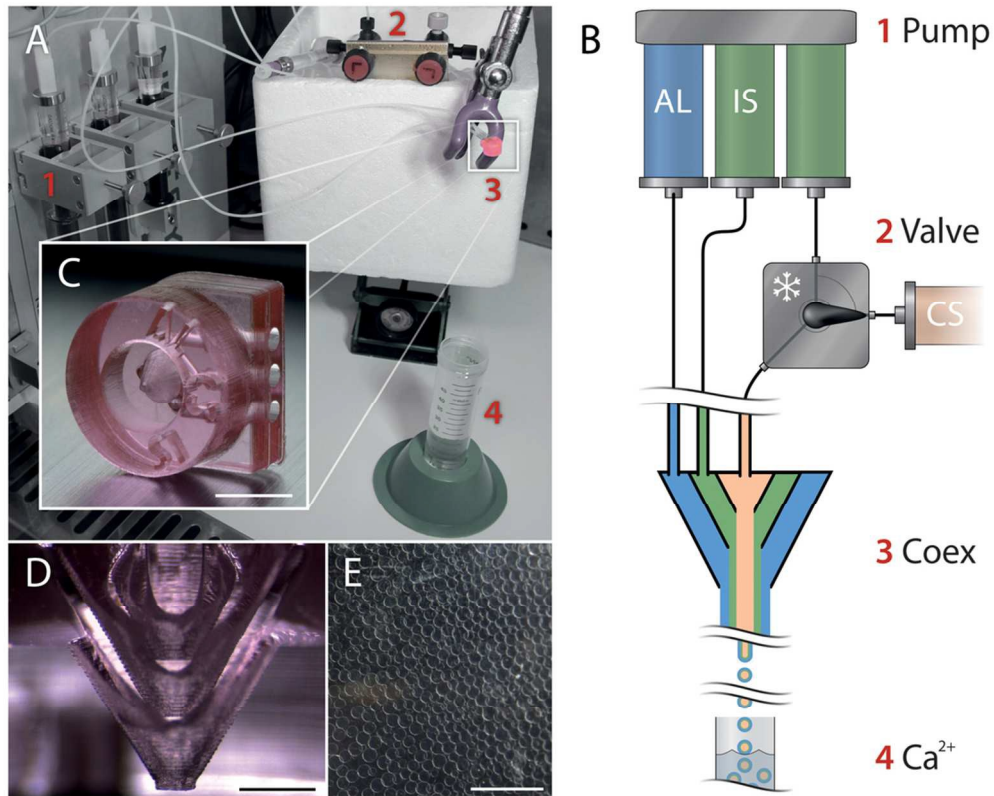
646x1073mm (72 x 72 DPI)

Fig. 3: Principle and operation of the encapsulation set-up for the production of capsules coated internally with a Matrigel layer. A. Picture of the set-up. B. Diagram of the co-extrusion set-up; Pump: set of 3 syringe pumps for flow control, Valve: Home-made thermostated device for Matrigel injection. AL, Alginate Solution, IS, Intermediate Solution and CS, Cell Suspension. Coex: 3D printed co-extrusion device, Ca2+: calcium gelation bath. Here, cells suspension is supplemented with liquid Matrigel. C. Photograph of the 3D printed co-extrusion device, scale bar 5mm, D. Close-up view of the co-extrusion device cut through the tip to display the internal circuitry, scale bar 500µm. E. Photograph of alginate capsules generated with the set-up shown in A, scale bar 1mm.
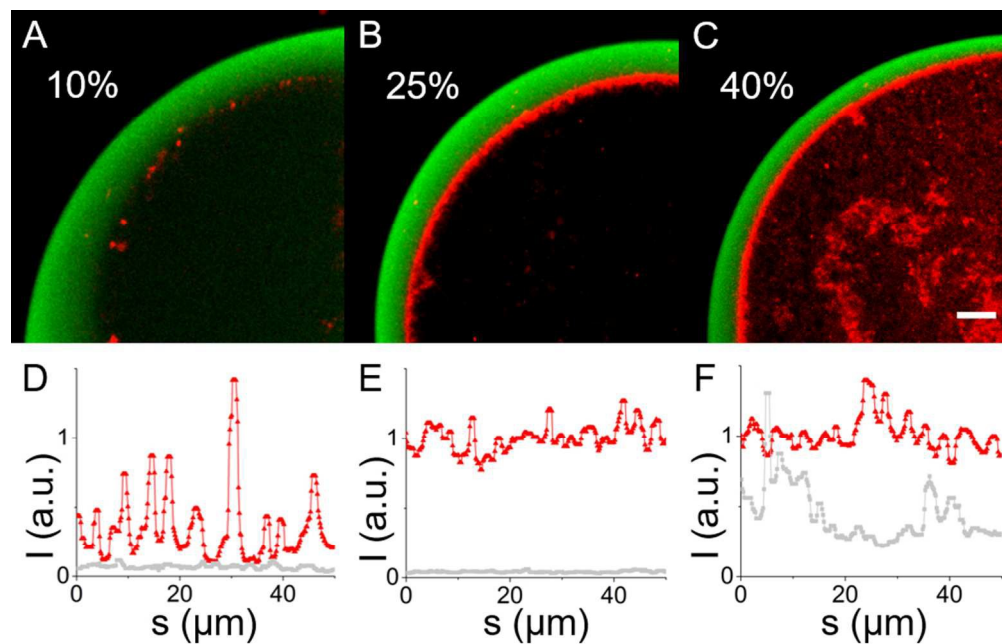95x77mm (300 x 300 DPI)
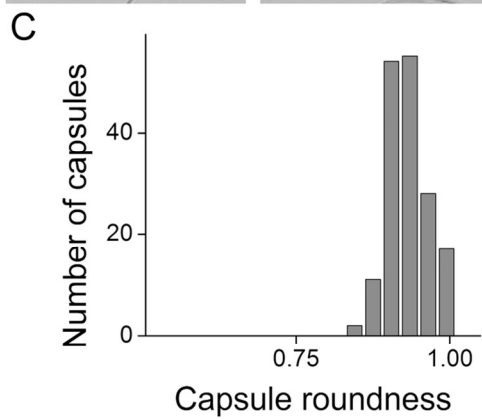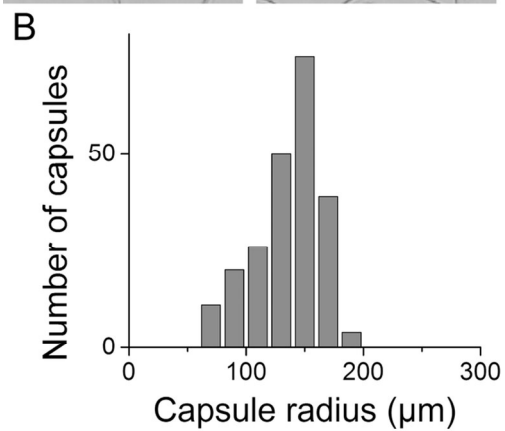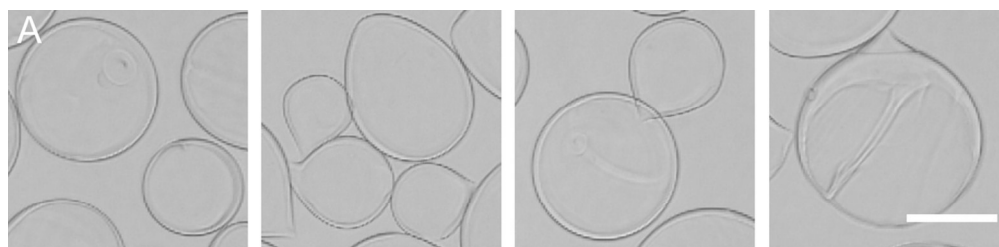
115x77mm (300 x 300 DPI)

Fig. 5: Conditions for the formation of Matrigel-coated capsules. A-C. Confocal images of the equatorial plane of a representative capsule formed with: 10% (A), 25% (B), and 40% (C) of Matrigel as volume fractions in the core. Scale bar 10µm. D-F Curvilinear scans along circular contours through the Matrigel layer (in red) and at mid-distance from the center (in grey) providing plots of the normalized fluorescence intensity I as a function of the curvilinear coordinate s respectively at 10% (D), 25% (E), 40% (F) of Matrigel as volume fractions in the core.
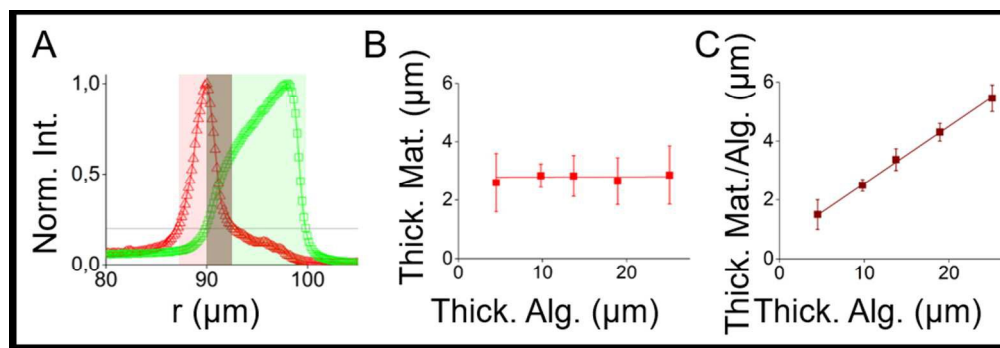170x109mm (150 x 150 DPI)

Figure 6: Characterization of the Matrigel layer. A. Averaged radial profiles measured from confocal images of a capsule for the Matrigel layer (red) and the alginate shell (green). Shaded areas underline the extent of the pure Matrigel layer inside the capsule (red), the thickness of the alginate shell (green) and the zone in which Matrigel and Alginate overlap (brown), suggesting the formation of interpenetrating polymer networks. B. Thickness of the pure Matrigel layer versus thickness of the alginate shell. C. Thickness of the Matrigel/alginate intermixed layer (brown in A) versus thickness of the alginate shell (green in A). Measured thicknesses in B and C are taken for fluorescence intensity I>0.2 Imax.
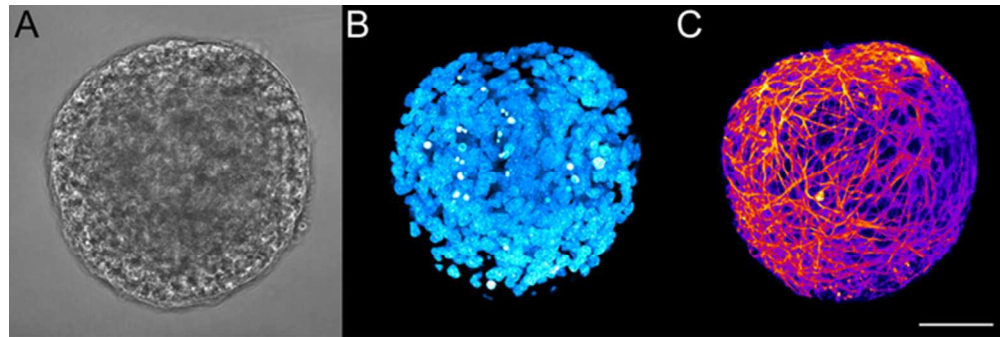172x59mm (150 x 150 DPI)

Fig. 7: Micrographs of a fixed neuronal capsule by bright field microscopy (A) and by fluorescence confocal microscopy (B-C) with DAPI staining of the nuclei (B) and with tubulin subunit Beta3 staining of mature neurites (C). Note that PFA treatment for fixation dissolves the alginate gel (not visible here). Scale bar 50μm
56x18mm (300 x 300 DPI)